Nanoscale Advances

ROYAL SOCIETY OF CHEMISTRY

PAPER

View Article Online
View Journal | View Issue

Cite this: *Nanoscale Adv.*, 2025, **7**, 6220

Nanoplastics from single-use polyethylene terephthalate bottles impair the functionality of human gut-dwelling *Lactobacillus rhamnosus* and induce toxicity in human cells†

Prashant Sharma, [a] Sakshi Dagariya,[a] Gurvinder Singh, [bc] Dinesh Kumar [bc] and Manish Singh *[a]

Plastic pollution from single-use plastic bottles (SUPBs) generates micro and nanoplastics (NPs), raising concerns about their interactions with biological systems and potential health effects. While NPs have been detected in the human body, raising serious concerns about their possible effects on health, a clear understanding of how NPs interact with key biological systems in the human body is still lacking. In this study, NPs were synthesized from polyethylene terephthalate (PET) bottles to closely mimic real-world exposure. Their effects were investigated using a comprehensive, multi-model approach integrating three biologically relevant systems: *Lactobacillus rhamnosus* as a representative gut probiotic, red blood cells to assess blood compatibility, and A549 human epithelial cells to model general cellular responses. By evaluating the same nanoplastic particles across these systems, the study offers a realistic and mechanistic view of how such particles may impact human health. The synthesized PET bottle-derived NPs (PBNPs), ranging from 50 to 850 nm, closely mimicked naturally occurring environmental NPs. Exposure to PBNPs led to a dose- and time-dependent reduction in *L. rhamnosus* viability, with pronounced effects after 16 days. Growth kinetics revealed impaired proliferation at higher concentrations, and confocal microscopy confirmed membrane damage. PBNPs also reduced antioxidant activity, antibacterial activity and increased biofilm formation, autoaggregation, and antibiotic sensitivity. Adhesion assays showed reduced bacterial attachment to colon epithelial cells, indicating disrupted colonization. Gene expression analysis reflected oxidative stress responses, while metabolomic profiling revealed alterations in energy, amino acid, and membrane lipid metabolism. In RBCs, PBNP exposure at higher concentrations induced morphological changes consistent with membrane destabilization, indicating potential hemolytic toxicity. In A549 cells, short-term exposure showed minimal effects, but prolonged exposure led to reduced viability, accompanied by DNA damage and increased expression of apoptotic, oxidative stress, and inflammatory markers. Metabolomic profiling revealed alterations in glucose metabolism, amino acid balance, and lipid-associated pathways. Ames testing showed no direct mutagenicity, but metabolic activation increased mutagenic potential, suggesting bioactivation-dependent genotoxicity. These findings demonstrate how real-world NPs can impair probiotic function, damage blood cells, and induce cellular toxicity, underscoring the need for deeper mechanistic understanding and appropriate regulatory strategies.

Received 22nd June 2025
Accepted 23rd July 2025

DOI: 10.1039/d5na00613a

rsc.li/nanoscale-advances

1. Introduction

Plastics, known for their easy adaptability, affordability, and unique mechanical properties, have become an integral part of our modern life. Over the decades, the widespread production and consumption of plastics have significantly improved the quality of life. However, their extensive use, coupled with improper disposal, has led to a surge in environmental pollution, raising global concerns. Plastics, being stable polymers, persist in the environment and do not biodegrade, however they undergo gradual degradation into smaller particles, ultimately

[a]*Chemical Biology Unit, Institute of Nano Science and Technology, Knowledge City, Sector-81, Mohali 140306, Punjab, India. E-mail: manish@inst.ac.in*

[b]*Department of Advanced Spectroscopy and Imaging, Centre of Biomedical Research (CBMR), SGPGIMS Campus, Raibareli Road, Lucknow 226014, Uttar Pradesh, India*

[c]*Academy of Scientific and Innovative Research (AcSIR), Ghaziabad, 201002, Uttar Pradesh, India*

† Electronic supplementary information (ESI) available: Additional experimental details, materials, and methods, characterization results of PBNPs, metabolomic volcano plot, and spectra bin images. See DOI: https://doi.org/10.1039/d5na00613a

forming microplastics (1–5 mm) and nanoplastics (1–1000 nm).[1,2]

NPs are now ubiquitous, contaminating terrestrial, aquatic, and aerial ecosystems, as well as soil, sediments, drinking water, and food supplies.[1,3] They enter the food chain through ingestion, inhalation, and dermal contact, posing significant environmental and health risks. Due to their small size, high surface area-to-volume ratio, and unique chemical properties, NPs exhibit greater toxicity than microplastics.[3,4] As they are reported to permeate through biological barriers, such as the gut and blood–brain barriers, they may lead to genotoxic, inflammatory, and even carcinogenic effects as well.[5] While some existing studies have documented the oxidative stress, immune system activation, and DNA damage caused by NPs, a comprehensive understanding of the toxicological outcomes and the molecular mechanisms behind these effects, especially over the long term, is still lacking.[6]

Among the various plastic types contributing to this widespread contamination, polyethylene terephthalate (PET) is particularly concerning.[7] Commonly used in single-use items such as water bottles and food containers, PET degrades over time into nanoscale particles that persist in the environment.[3,8] Given its extensive presence in consumer products and its high likelihood of environmental release, PET-derived NPs serve as a relevant and realistic model for assessing potential biological interactions. Therefore, in this study, PET was chosen to simulate real-world exposure scenarios and to systematically investigate how such NPs influence living systems at multiple biological levels.

The novelty of this research lies in its exploration of a largely unexplored aspect of NPs toxicity along with their impact on the gut microbiome, with a particular focus on the probiotic activities of the beneficial endocommensal of human gut, *Lactobacillus rhamnosus* (*L. rhamnosus*). Although recent studies have shown that certain probiotic strains may mitigate the toxicity of micro- and NPs in animal or cellular systems, this protective effect is often attributed to their capacity to adsorb or trap NPs, possibly through biofilm formation, which reduces the particles' availability to host cells.[9–11] However, these studies have primarily focused on the host-protective aspect, with limited attention to the direct effects of NPs on the probiotic bacteria themselves. In particular, under prolonged exposure, it remains unclear how such interactions affect the physiology, metabolic activity, and functionality of beneficial microbes. This gap underscores the need to investigate how environmentally relevant NPs influence probiotics at both structural and metabolic levels. Some preliminary studies have raised concerns that NPs may disrupt the gut microbiome; however, the specific effects on beneficial bacteria and the long-term implications for gut health and overall well-being remain poorly understood.

Building on these concerns, the present study set out to examine these issues more closely by evaluating the biological effects of PET bottle-derived NPs. To do this, NPs were synthesized from single-use PET bottles using an oil-in-water nanoemulsion technique, which provides advantages such as precise size control and scalability over conventional methods. These particles were characterized using a range of analytical tools, including dynamic light scattering (DLS), field emission scanning electron microscopy (FESEM), transmission electron microscopy (TEM), atomic force microscopy (AFM), Raman spectroscopy, and Fourier-transform infrared (FTIR) spectroscopy. Together, these methods offered a comprehensive profile of the NPs' size, surface morphology, and chemical structure. Following synthesis and characterization, the long-term biological effects of NPs were evaluated using a multi-model approach targeting three biologically relevant systems: probiotic bacteria (*L. rhamnosus*), red blood cells, and A549 human epithelial cells. This design was intended to reflect different levels of biological complexity and realistic exposure routes in humans.

In the bacterial model, *L. rhamnosus* was exposed to NPs for 16 days to mimic chronic environmental contact. To evaluate basic survival and proliferation, bacterial viability and growth kinetics were measured over time. Functional assays were then conducted to assess biofilm formation, auto-aggregation, and adhesion capacity—factors essential for effective colonization and probiotic functionality in the gut environment. Antibiotic susceptibility profiling was included to examine whether NP exposure influenced bacterial resistance patterns, which could have clinical implications. To assess oxidative stress responses, antioxidant potential was measured using the DPPH radical scavenging assay. To uncover cellular stress mechanisms and biochemical alterations, gene expression analysis was performed to evaluate the transcriptional response to NP exposure, while NMR-based metabolomic profiling was employed to identify shifts in metabolic pathways indicative of long-term functional disruption.

To evaluate the cellular and molecular effects of NPs in human systems, two complementary mammalian models were employed. A549 epithelial cells were used to represent the respiratory epithelium, where cell viability assays were performed to determine general cytotoxicity. Genotoxicity was assessed using both comet and Ames assays, providing a comprehensive analysis of DNA damage at both the cellular and mutagenic levels. To assess membrane integrity and hemocompatibility, red blood cells were exposed to NPs, and the degree of hemolysis was measured. Beyond these primary toxicological endpoints, molecular alterations were further investigated through gene expression analysis and metabolomic profiling in A549 cells to capture stress responses and biochemical changes associated with prolonged exposure.

Overall, this study bridges a critical gap between environmental NP exposure and its biological consequences, offering valuable insights into potential health risks by simultaneously addressing effects on probiotics, red blood cells, and human epithelial cells.

2. Methodology

2.1. Synthesis and characterization of PET bottle-derived NPs (PBNPs)

NPs were synthesized from single-use PET bottles using a nanoemulsion technique, and their characterization was performed using DLS, SEM, TEM, AFM, Raman, and FTIR

spectroscopy. Detailed methods are provided in Section 1.2 of the ESI.†

2.2. Culture and exposure of *L. rhamnosus* to PBNPs

L. rhamnosus was cultured in MRS medium and exposed to PBNPs at concentrations of 25, 50, and 100 μg mL^{-1} (rationale for the dose selection given in the ESI Section 1.3†) for 16 days to mimic multi-generational exposure. Refer to Sections 1.4.1 and 1.4.2 of ESI for detailed experimental design.†

2.3. Bacterial viability, growth kinetics, membrane permeability and morphology

The impact of PBNPs on bacterial viability was assessed at multiple time points using CFU counting. After exposure, growth kinetics was measured by monitoring optical density at different time points, and membrane permeability was evaluated using DAPI/PI staining. The morphology of bacteria was observed by FESEM. See Sections 1.4.3, 1.4.4, 1.4.5 and 1.4.6 respectively of the ESI for protocol.†

2.4. Biofilm formation and autoaggregation assays

The effect of PBNPs on biofilm formation and autoaggregation was evaluated using crystal violet staining and optical density measurements, respectively. Detailed methods are provided in Sections 1.4.7 and 1.4.8 respectively of the ESI.†

2.5. Antibiotic susceptibility, antioxidant activity, antibacterial activity and cell adhesion assay

Antibiotic susceptibility, antioxidant activity, antibacterial activity and adhesive potential to mammalian cells were analyzed using the zone of inhibition assay, DPPH assay, and established cell adhesion assay, respectively. Detailed procedures are provided in Sections 1.4.9, 1.4.10, 1.4.11 and 1.4.12 of the ESI.†

2.6. Gene expression and metabolomic analysis

Gene expression changes post-PBNP exposure were evaluated by qPCR, and metabolomic profiles were analysed using NMR. Detailed methodologies are described in Section 1.4.13 and 1.4.14 of the ESI.†

2.7. Impact of PBNPs on mammalian cells

Hemolysis, cell viability, DNA damage assays, gene expression and metabolomic analysis were conducted to assess PBNPs' toxicity. Refer to Section 1.5 of the ESI for experimental details.†

2.8. Mutagenicity assessment using the Ames test

The mutagenic potential of PBNPs was evaluated using the Ames test, following standard protocols. *Salmonella typhimurium* strains MTCC 1252 (TA100) were used in the presence and absence of the S9 metabolic activation system to assess the mutagenicity of both metabolized and unmetabolized PBNPs. Detailed experimental procedures and control data are provided in Section 1.6 of the ESI.†

2.9. Statistical analysis

Statistical analyses were performed using GraphPad Prism 9.0, with appropriate tests for each dataset. Metabolomic analysis was conducted using MetaboAnalyst, including univariate analysis and ROC curve evaluation. Detailed methods are in Section 1.7 of the ESI.†

3. Results

3.1. Characterization of PBNPs

The synthesized PBNPs had an average hydrodynamic diameter of 322 nm (PDI = 0.262) (ESI Fig. 3i and h†) as determined by DLS, with size distributions ranging from 120 to 600 nm. SEM, TEM, and AFM revealed average sizes of 280 nm, 299 nm, and 320 nm, respectively (ESI Fig. 3a–f†), with non-uniform shapes and distributions ranging from 50 to 850 nm in size. HRTEM confirmed a lattice fringe spacing of 0.33 nm, indicating the crystalline nature (ESI Fig. 3g and h†). The size and morphology closely resemble naturally occurring NPs, making these PBNPs suitable for further studies.[12] To assess whether the synthesis process introduces any chemical modifications to PBNPs due to exposure to various solvents and reagents, Raman and FTIR spectroscopy were conducted on both the original PET fragments and the synthesized PBNPs. As shown in ESI Fig. 3j and k,† the spectral profiles exhibit no significant shifts in characteristic peaks between the two, indicating that the chemical structure of the PBNPs remains largely unaltered. The strong similarity in both Raman and FTIR spectra suggests that the chemical composition of the PBNPs closely matches that of the original SUPB fragments, with no major changes occurred during synthesis. These findings confirm that the structural integrity of the original polymer is preserved, ensuring that the resulting NPs remain environmentally relevant for further biological investigations.

3.2. Effects of PBNPs on the probiotic health and functionality of *L. rhamnosus*

The effects of NPs on the probiotic strain *L. rhamnosus* were assessed through a series of assays evaluating viability, biofilm formation, autoaggregation, adhesion, antioxidant activity, gene expression and metabolic profiling. Exposure to NPs caused significant alterations in probiotic functionality, with dose-dependent impacts on cellular behavior and metabolic activity. Below, we detail the specific observations under each parameter.

3.2.1. Time-dependent effects of PBNPs on bacterial viability. The impact of NPs on the viability of *L. rhamnosus* was evaluated over a 16-day exposure period using the colony count method, viability was assessed at various time points such as after the exposure of 1 day, 4 days, 8 days and 16 days (Fig. 1a–d). The results revealed a clear time- and dose-dependent reduction in bacterial viability. After 24 h and 4 days exposures, no significant changes in the bacterial viability were observed at any tested concentrations (25, 50, and 100 μg mL^{-1}). After 8 days exposure, a substantial dose dependent decline in the bacterial viability was evident, however it was statistically

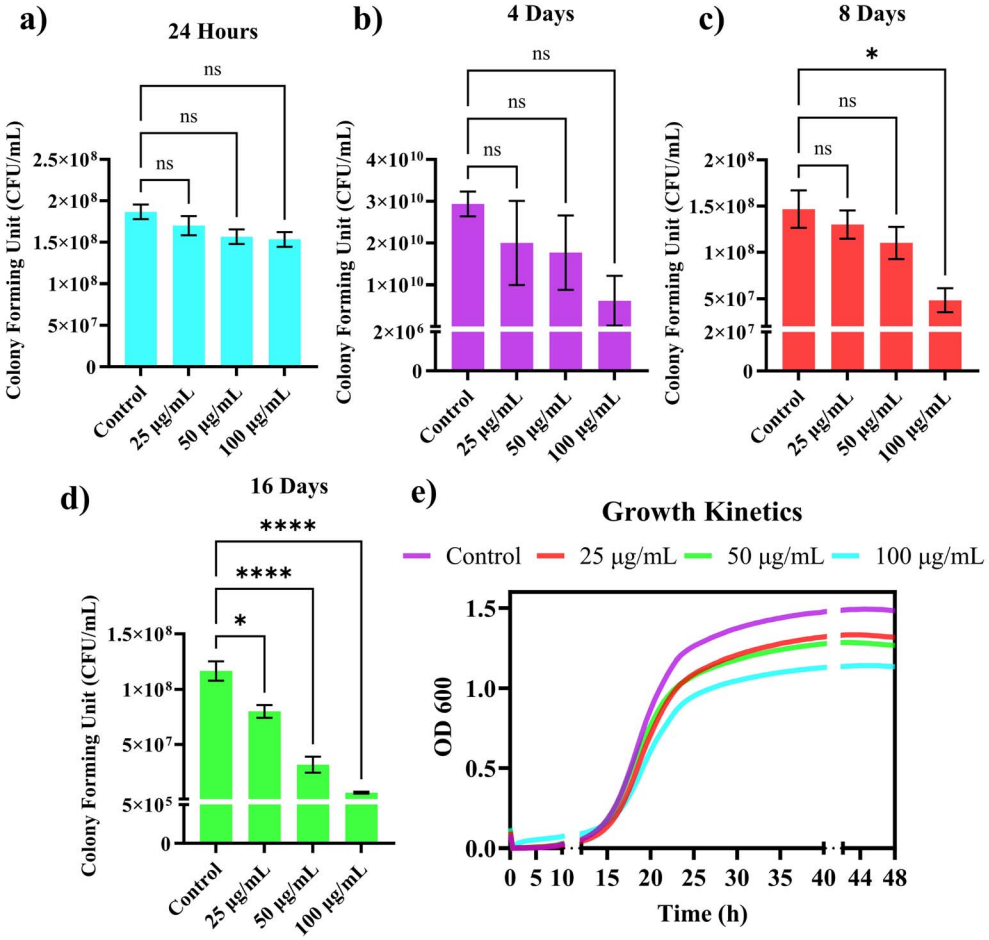

Fig. 1 Effects of PBNPs on *L. rhamnosus* viability, and growth kinetics. (a–d) CFU mL^{-1} analysis at different time points. (e) OD600 measurements of bacterial growth up to 48 h.

significant only at the highest concentration (100 µg mL^{-1}), whereas lower concentrations (25 and 50 µg mL^{-1}) did not show significant effects. After 16 days exposure, the decline was much more prominent and statistically significant at all test concentrations demonstrating the compounding impact of prolonged exposure. These findings reveal the progressive and concentration-dependent disruption of bacterial viability induced by NP exposure over time, underscoring the greater adverse effects with higher doses and extended exposure periods.

3.2.2. Effect on growth kinetics following prolonged exposure. The growth kinetics of *L. rhamnosus* exposed to 25, 50, and 100 µg mL^{-1} concentrations of NPs for 16 days were assessed by monitoring changes in optical density (OD600) over time. Fig. 1e shows that the control group exhibited the typical growth curve, with a steady increase in OD600 values, indicating healthy bacterial growth. However, cultures exposed to NPs displayed a clear disruption in the lag phase of growth kinetics. At concentrations of 50 and 100 µg mL^{-1}, the bacterial growth rate was significantly slower compared to the control group, as evidenced by the lower OD600 values. These cultures showed delayed growth and reduced overall growth compared to the control, with the higher concentrations (50 and 100 µg mL^{-1}) having a more pronounced effect. These results indicate that NP exposure impairs the growth kinetics of *L. rhamnosus*, with higher concentrations causing a more significant disruption in growth dynamics.

3.2.3. Impact on bacterial membrane integrity: confocal imaging. To further evaluate the effects of NPs over membrane integrity of bacterial cells, *L. rhamnosus* cultures exposed to NPs at various concentrations (25, 50, and 100 µg mL^{-1}) for 16 days were subjected to confocal microscopy analysis (Fig. 2). The cells were stained with Propidium Iodide (PI) and DAPI to assess cell membrane integrity and overall cell health. In the control group, bacterial cells appeared intact, as indicated by minimal PI staining (red fluorescence). However, as the NP concentration increased, the number of cells with compromised membranes (indicated by strong PI staining) also increased, especially at 50 and 100 µg mL^{-1} concentrations. The results suggest that NPs may disrupt the cell membrane integrity of *L. rhamnosus*, leading to the increased cell damage at higher concentrations.

3.2.4. Effect on bacterial morphology and size. Field emission scanning electron microscopy (FESEM) images

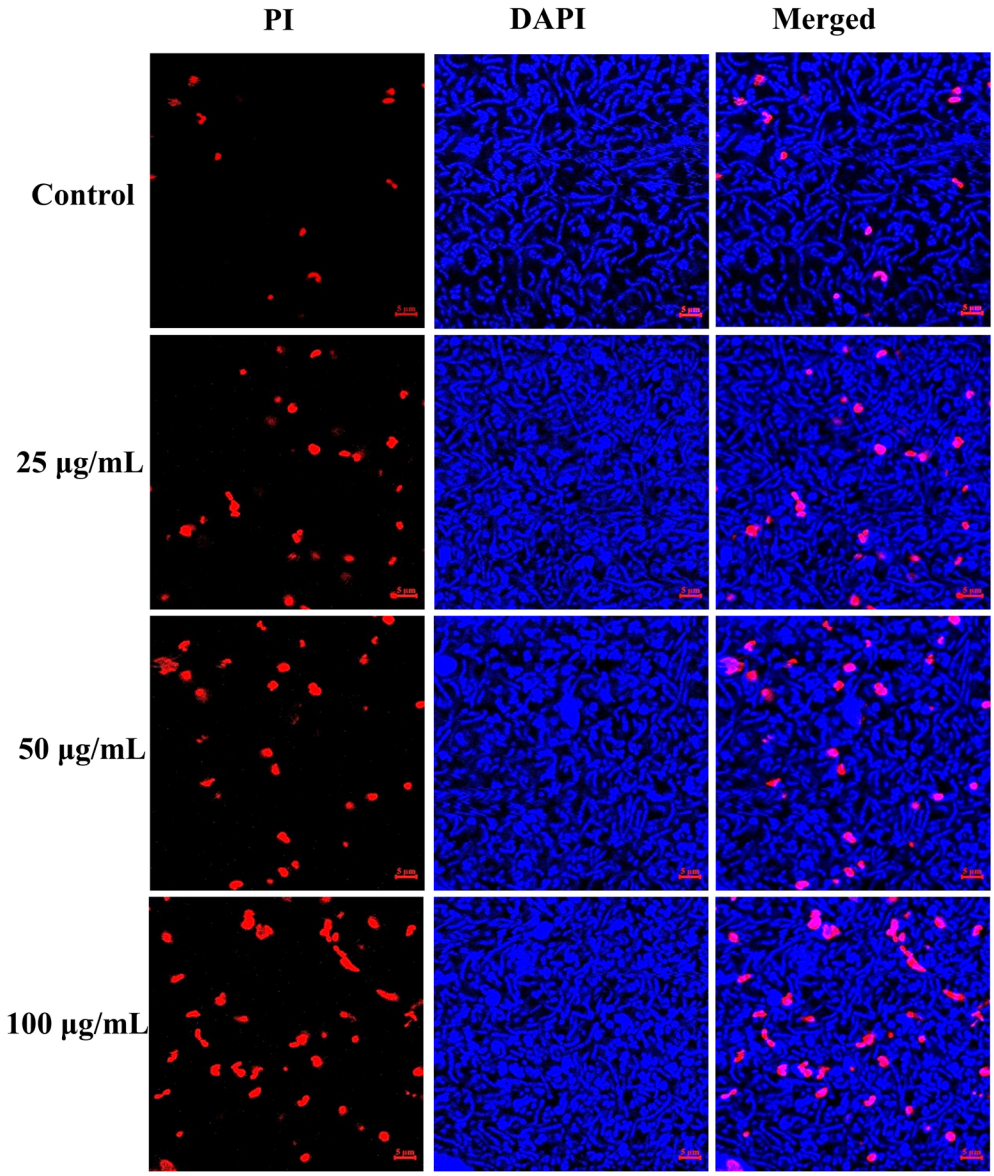

Fig. 2 DAPI/PI staining of *L. rhamnosus* demonstrating the impact on membrane integrity following 16-day exposure to PBNPs.

(Fig. 3a) revealed distinct changes in the morphology and size of *L. rhamnosus* cells after 16 days of exposure to PBNPs at concentrations of 25, 50, and 100 μg mL^{-1}. Compared to the control, bacterial cells exposed to PBNPs exhibited larger cell sizes, as indicated by the measurements (Fig. 3b). Exposure to increasing concentrations of PBNPs led to a statistically significant and dose dependent increase in the average bacterial size as compared to that of control. The size increased from 1.29 μm in the control group to 1.44 μm, 1.54 μm, and 1.76 μm at concentrations of 25, 50, and 100 μg mL^{-1} PBNPs, respectively (Fig. 3b). Histograms of bacterial size distribution (Fig. 3c) demonstrated a shift towards larger cell sizes in response to PBNPs exposure. In the control group, the majority of cells were distributed around 1.29 μm, whereas in treated groups, the distributions shifted towards higher size ranges, with a notable broadening of the distribution at 100 μg mL^{-1} PBNPs concentration.

3.2.5. Effect on antibiotic susceptibility. Antibiotic susceptibility testing demonstrated a significant impact of PBNPs exposure on the antibiotic sensitivity of *L. rhamnosus* to the antibiotics like kanamycin, gentamicin, and ampicillin. For kanamycin and ampicillin, the zones of inhibition were significantly increased across all PBNPs concentrations (Fig. 3d). In contrast, the zone of inhibition for gentamicin showed significant increase only at the 100 μg mL^{-1} concentration of PBNPs. These results demonstrate that bacterial exposure to PBNPs leads to altered antibiotic susceptibility. Visual comparison of the antibiotic susceptibility plates (Fig. 3e) corroborated the quantitative findings, showing consistent trends. Specifically, kanamycin, gentamicin, and ampicillin exhibited larger zones of inhibition in PBNP-exposed groups compared to the control,

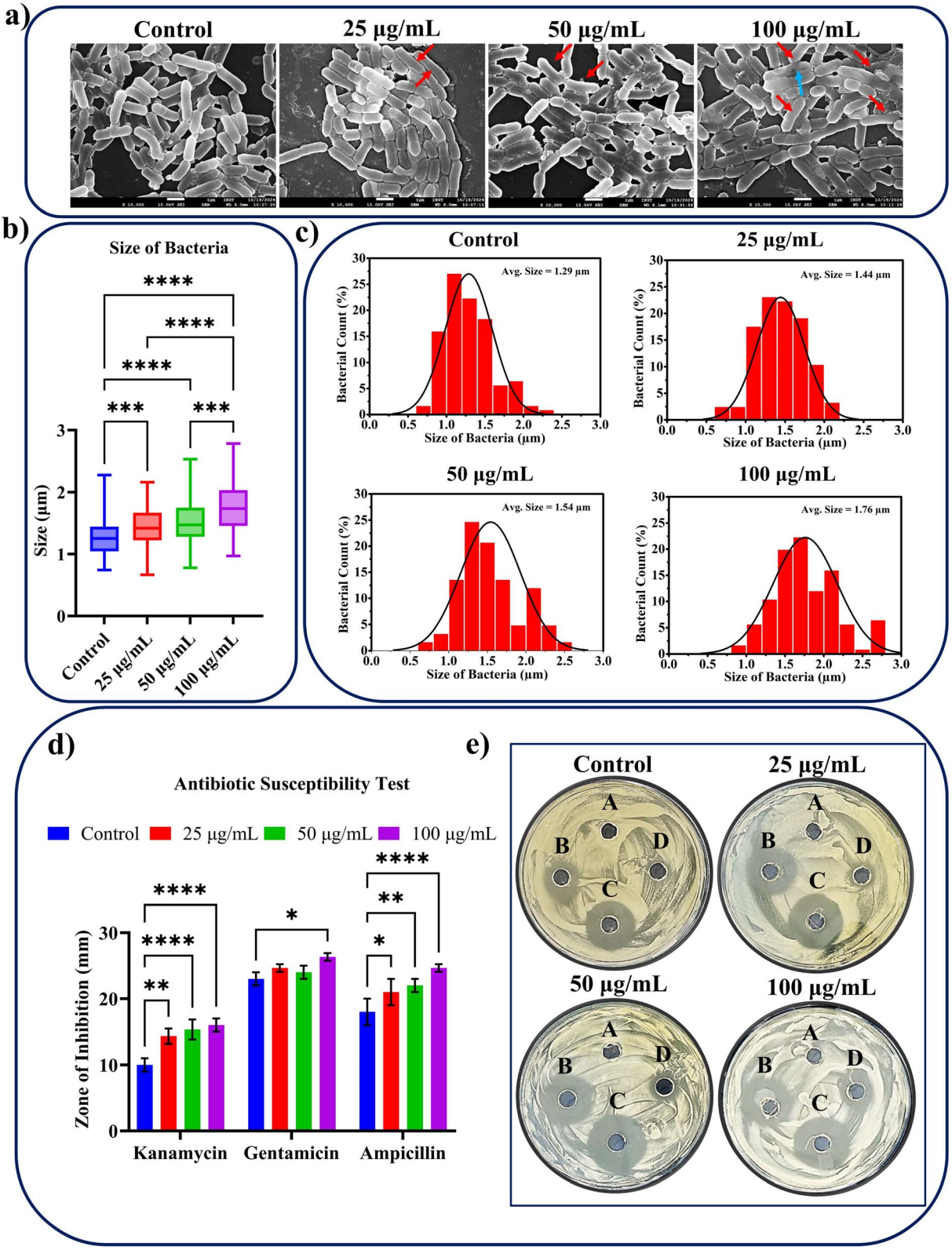

Fig. 3 Effects of PBNPs on *L. rhamnosus* morphology, size distribution, and antibiotic susceptibility after 16 days exposure. (a) FESEM images showing morphological changes and enlarged cell sizes with increasing PBNP concentrations. (b) Box plot depicting a dose-dependent increase in bacterial size. (c) Histograms illustrating size distribution. (d) Antibiotic susceptibility test showing altered inhibition zones for kanamycin, gentamicin, and ampicillin. (e) Representative agar plates visualizing inhibition zones across different treatment groups.

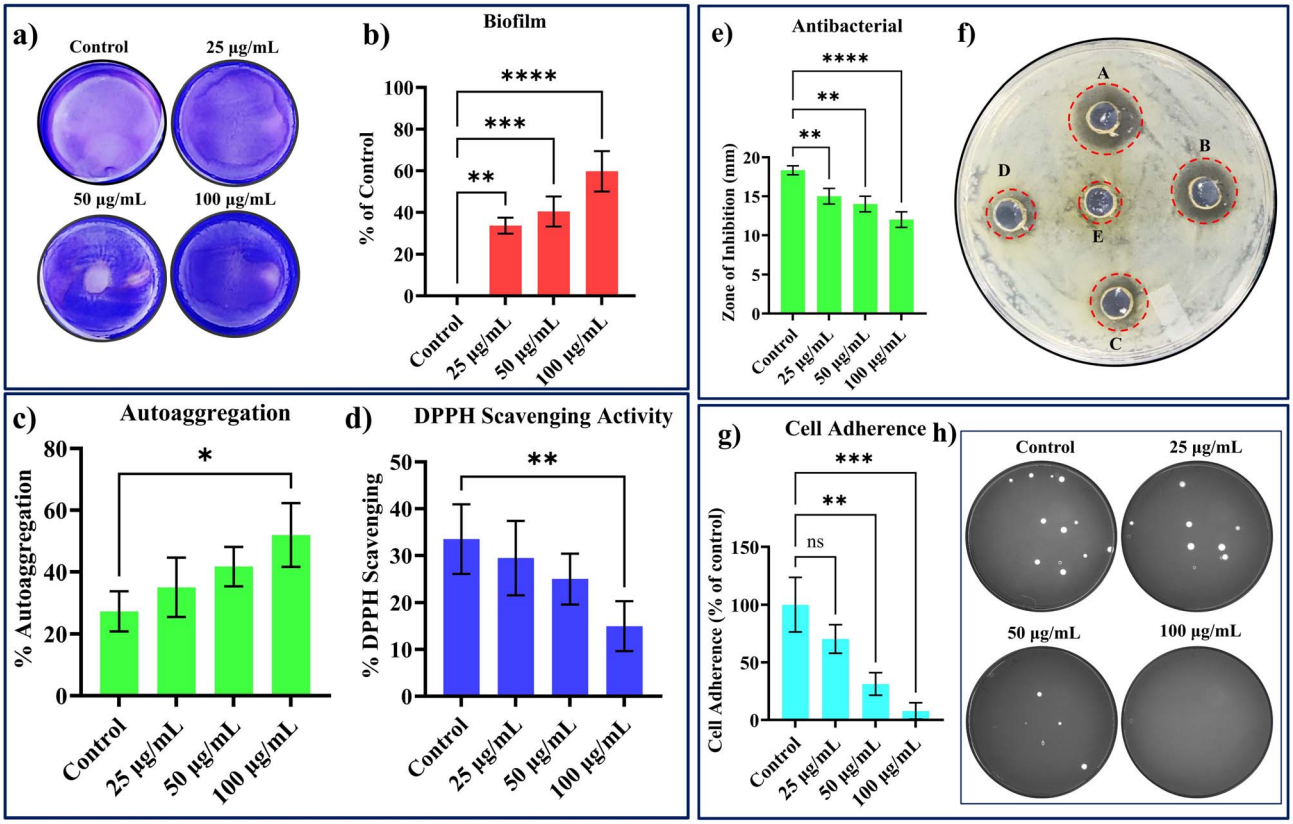

Fig. 4 Effects of PBNPs on biofilm formation, autoaggregation, antioxidant activity, antibacterial activity, and adhesion ability of *L. rhamnosus* after 16 days of exposure. (a) Crystal violet-stained biofilms at different PBNPs concentrations. (b) Quantitative analysis of biofilm formation. (c) Autoaggregation percentage of *L. rhamnosus* at varying PBNPs concentrations. (d) DPPH scavenging activity of *L. rhamnosus* after PBNP exposure. (e) Antibacterial activity against *Pseudomonas aeruginosa*, measured from inhibition zones. (f) Representative agar plate showing inhibition zones across PBNPs concentrations. (g) Adhesion ability of *L. rhamnosus* to HCT 116 cells, expressed as a percentage relative to the control. (h) Representative images showing bacterial adherence under control and PBNPs-treated conditions.

with the most pronounced effects observed at higher concentrations of 50 and 100 µg mL^{-1} for kanamycin and ampicillin, and at 100 µg mL^{-1} for gentamicin.

3.2.6. Effects on biofilm formation. After 16 days of exposure to PBNPs, *L. rhamnosus* showed a dose-dependent increase in biofilm formation. Crystal violet staining revealed progressively enhanced biofilm density at concentrations of 25, 50, and 100 µg mL^{-1} as compared to the control (Fig. 4a). Quantitative analysis indicated that biofilm formation was increased by approximately 33% at 25 µg mL^{-1}, 40% at 50 µg mL^{-1}, and 60% at 100 µg mL^{-1} (Fig. 4b). The increase was statistically significant at all concentrations, with the most pronounced effect observed at 100 µg mL^{-1}.

3.2.7. Impact on bacterial autoaggregation. The autoaggregation ability of *L. rhamnosus* was increased following the exposure to various doses of PBNPs. Autoaggregation percentages were higher at all tested concentrations compared to the control, with the greatest increase observed at 100 µg mL^{-1} (Fig. 4c). This increase was statistically significant, indicating a clear enhancement of bacterial aggregation with increasing PBNP concentrations.

3.2.8. Impact on antioxidant activity. The DPPH scavenging activity of *L. rhamnosus* was significantly reduced after 16 days of exposure to PBNPs. The data indicate a consistent decline in scavenging activity as the concentration of PBNPs exposure was increased. However, the values were statistically significant only at 100 µg mL^{-1} PBNPs concentration (Fig. 4d).

3.2.9. Impact on antibacterial activity. The antibacterial activity of *L. rhamnosus* exposed to PBNPs for 16 days was assessed against *Pseudomonas aeruginosa* (*P. aeruginosa*) using the zone of inhibition assay (Fig. 4e and f). A dose-dependent reduction in antibacterial activity was observed. The control (unexposed *L. rhamnosus* labeled A) exhibited a zone of inhibition of approximately 18 mm. Exposure to 25 µg mL^{-1} PBNPs (labeled B) resulted in a reduction to 15 mm, which further decreased to 14 mm at 50 µg mL^{-1} (labeled C) and 12 mm at 100 µg mL^{-1} (labeled D). MRS media alone (labeled E) exhibited no inhibition zone, serving as a negative control. These results demonstrate that increasing concentrations of PBNPs significantly reduced the antibacterial activity of *L. rhamnosus* against *P. aeruginosa*. Representative agar plates (Fig. 4f) visually highlight this dose-dependent decrease in antibacterial activity.

3.2.10. Impact on cell adherence. The ability of *L. rhamnosus* to adhere to HCT 116 colon epithelial cells was evaluated after 16 days of PBNPs exposure (Fig. 4g and h). The results revealed a significant, concentration-dependent reduction in

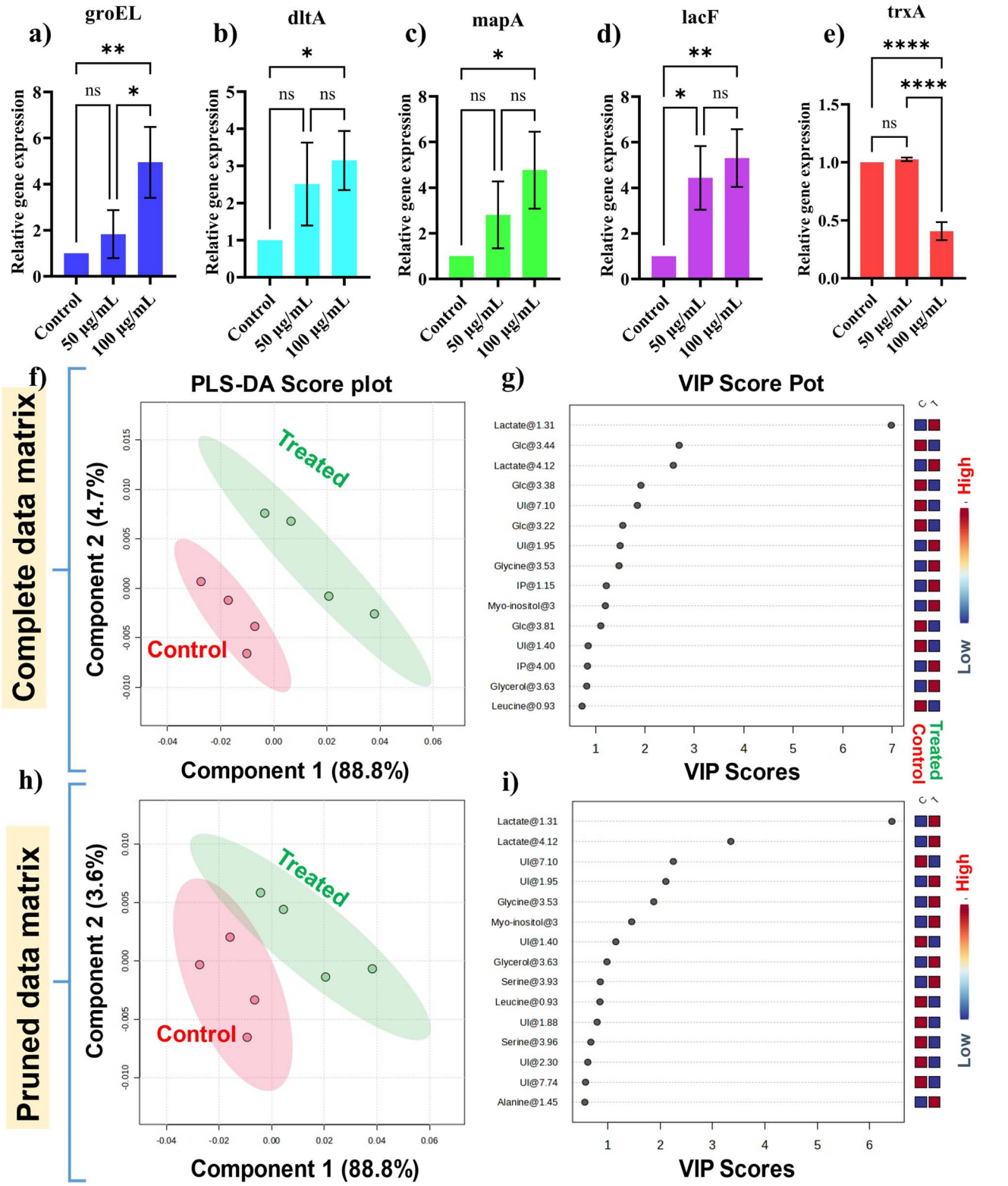

Fig. 5 Gene expression analysis and metabolomic profiling of *L. rhamnosus* after 16 days of PBNPs exposure. (a) *groEL* (stress response), (b) *dltA* (cell wall integrity), (c) *mapA* (bacterial adherence), (d) *lacF* (carbohydrate metabolism), and (e) *trxA* (redox regulation) gene expression levels at 50 µg mL^{-1} and 100 µg mL^{-1} PBNPs exposure. (f) PLS-DA score plot for the complete data matrix illustrating distinct clustering between control (red) and treated (green) groups. (g) VIP score plot for complete data matrix, highlighting significant metabolites contributing to group differentiation. (h) PLS-DA score plot for the pruned data matrix with clustering patterns. (i) VIP score plot for the pruned matrix, highlighting significant metabolites contributing to group differentiation.

bacterial adherence to the HCT 116 cell line. At 25 μg mL^{-1}, adherence level was ~70% of the control level, however it was not statistically significant, while at 50 μg mL^{-1} and 100 μg mL^{-1} PBNPs exposure, adherence was significantly reduced to ~31% and ~8% of the control, respectively. Representative plate images (Fig. 4h) visually confirm this trend, demonstrating a marked decline in bacterial adherence to HCT 116 cells with increasing concentrations of PBNPs.

3.2.11. Effect on gene expressions. Gene expression analysis of *L. rhamnosus* exposed to PBNPs for 16 days revealed significant alterations in key genes (Fig. 5). The *groEL* gene, which is involved in stress response, exhibited a concentration-dependent upregulation. At 50 μg mL^{-1} PBNPs, its expression increased approximately 2-fold compared to the control, though this change was not statistically significant. However, at 100 μg mL^{-1}, a significant ~5-fold increase was observed (Fig. 5a).

Similarly, the *dltA* gene, which plays a role in cell wall integrity, showed a moderate upregulation. At 50 μg mL^{-1}, the expression increased by ~2.5-fold but did not reach statistical significance. However, at 100 μg mL^{-1}, a significant ~3-fold upregulation was observed (Fig. 5b). The *mapA* gene, associated with adherence and colonization, displayed a increase in expression upon PBNPs exposure, with a significant change detected only at 100 μg mL^{-1} (~4-fold) (Fig. 5c). Similarly, the *lacF* gene, which is involved in carbohydrate metabolism, exhibited remarkable upregulation. Its expression increased ~4-fold at 50 μg mL^{-1} and ~5-fold at 100 μg mL^{-1}, both of which were statistically significant (Fig. 5d). In contrast to these, the trxA gene, which is associated with redox regulation, was significantly downregulated in response to PBNP exposure at 100 μg mL^{-1} concentration. Expression level was unaffected at 50 μg mL^{-1} PBNP exposure, but reduced to ~0.5-fold of the control level at 100 μg mL^{-1} exposure concentration (Fig. 5e).

3.2.12. Impact on metabolites. The metabolomics analysis of *L. rhamnosus* treated with PBNPs (nanoplastics) revealed significant metabolic differences between the treated and control groups, as demonstrated by PLS-DA and VIP score analyses (Fig. 5f–i). The PLS-DA score plot for the complete data matrix displayed distinct clustering, with Component 1 explaining 88.8% of the variance and Component 2 contributing 4.7% (Fig. 5f). Validation metrics for the complete matrix were robust, with R^2 values ranging from 0.6118 to 0.99876 and Q^2 values from 0.29961 to 0.81187, indicating a well-fitted model with high predictive power. After pruning out the redundant regions dominated by glucose and lactate signals, the pruned data matrix maintained distinct group separation with Component 1 still explaining 88.8% of the variance and Component 2 contributing 3.6% (Fig. 5h). The pruned matrix validation parameters, although slightly reduced, were consistent, with R^2 values from 0.57053 to 0.99254 and Q^2 values ranging from 0.2451 to 0.54668, ensuring the reliability of the analysis (ESI Fig. 4a†). The VIP score analysis identified key metabolites contributing significantly to group separation in both the complete and pruned data matrices. For the complete matrix, glucose signals (Glc@3.22, Glc@3.38, Glc@3.44, Glc@3.81), lactate signals (Lactate@1.31, Lactate@4.12), glycine (Glycine@3.53), Myo-inositol (Myo-inositol@3), and unidentified metabolites (UI@7.10UI@1.95, UI@1.40) were highlighted with VIP scores >1.0% (Fig. 5g). The heatmap on the right shows that lactate, glycine, and myo-inositol were increased, while glucose levels were reduced. In the pruned data matrix, additional metabolites such as serine (Serine@3.96), glycerol (Glycerol@3.63) and leucine (Leucine@0.93) also emerged as significant contributors, further refining the metabolic profile of the treated samples (Fig. 5i). The heatmap on the right shows increased levels of serine and glycerol, while leucine levels were reduced.

The volcano plot (treated with respect to control) analysis corroborated these findings, indicating statistically significant downregulation of glucose (Glc@3.22, Glc@5.22, Glc@3.44) peaks in treated samples compared to controls (ESI Fig. 5†). The spectral bin analysis further confirmed these changes, with glucose peaks (Glc@3.22, Glc@3.38, Glc@3.44, Glc@5.21) and an unidentified metabolite (UI@1.88) showing significant alterations based on their $-\log 10$ (FDR·p) values (ESI Fig. 6†). Overall, the results from the complete and pruned data matrices consistently revealed significant differences in glucose, and other key metabolites such as lactate, and glycerol levels, alongside changes in amino acids such as glycine, serine, and leucine.

3.3. Effects of nanoplastics (PBNPs) on mammalian cells

This section presents the results of various *in vitro* assays conducted on mammalian cells to evaluate the effects of PBNPs. The findings include data on hemocompatibility (hemolysis), cytotoxicity (cell viability), genotoxicity (Ames and comet assays), gene expression changes, and metabolomic alterations. Each subsection reports the outcomes of the respective assays, highlighting the observable effects of PBNPs on the cellular integrity and function of A549 cells.

3.3.1. Effects on red blood cells. The hemolytic potential of PBNPs was assessed to evaluate their impact on red blood cells' (RBC) membrane integrity. Fig. 6a reveals that PBNPs concentrations of 25 μg mL^{-1} and 50 μg mL^{-1} induced negligible hemolysis (<2%), comparable to the control group. However, hemolysis increased at 100 μg mL^{-1}, exceeding 2%, indicating a concentration-dependent effect. Triton X-100 (0.1%) served as a positive control, inducing near-complete hemolysis, validating the assay's sensitivity. Corresponding visual observations in Fig. 6b corroborate these findings, with visibly clear supernatants for PBNPs concentrations and a distinctly red supernatant for 0.1% Triton X-100.

Microscopic examination further confirmed the hemolytic potential of PBNPs. As shown in Fig. 6c, RBCs in the control and low-concentration (25 μg mL^{-1}) groups maintained their characteristic biconcave shape, indicating preserved membrane integrity (Fig. 6c, indicated by green arrows). At 50 μg mL^{-1}, slight morphological alterations, such as changes in shape, were observed (Fig. 6c, indicated by blue arrows). At 100 μg mL^{-1}, severe deformations, including cell shrinkage and membrane disruption, became evident (blue arrows). Triton X-100 treatment caused complete lysis, with no intact cells visible (red arrow), affirming the destructive effects of membrane destabilization.

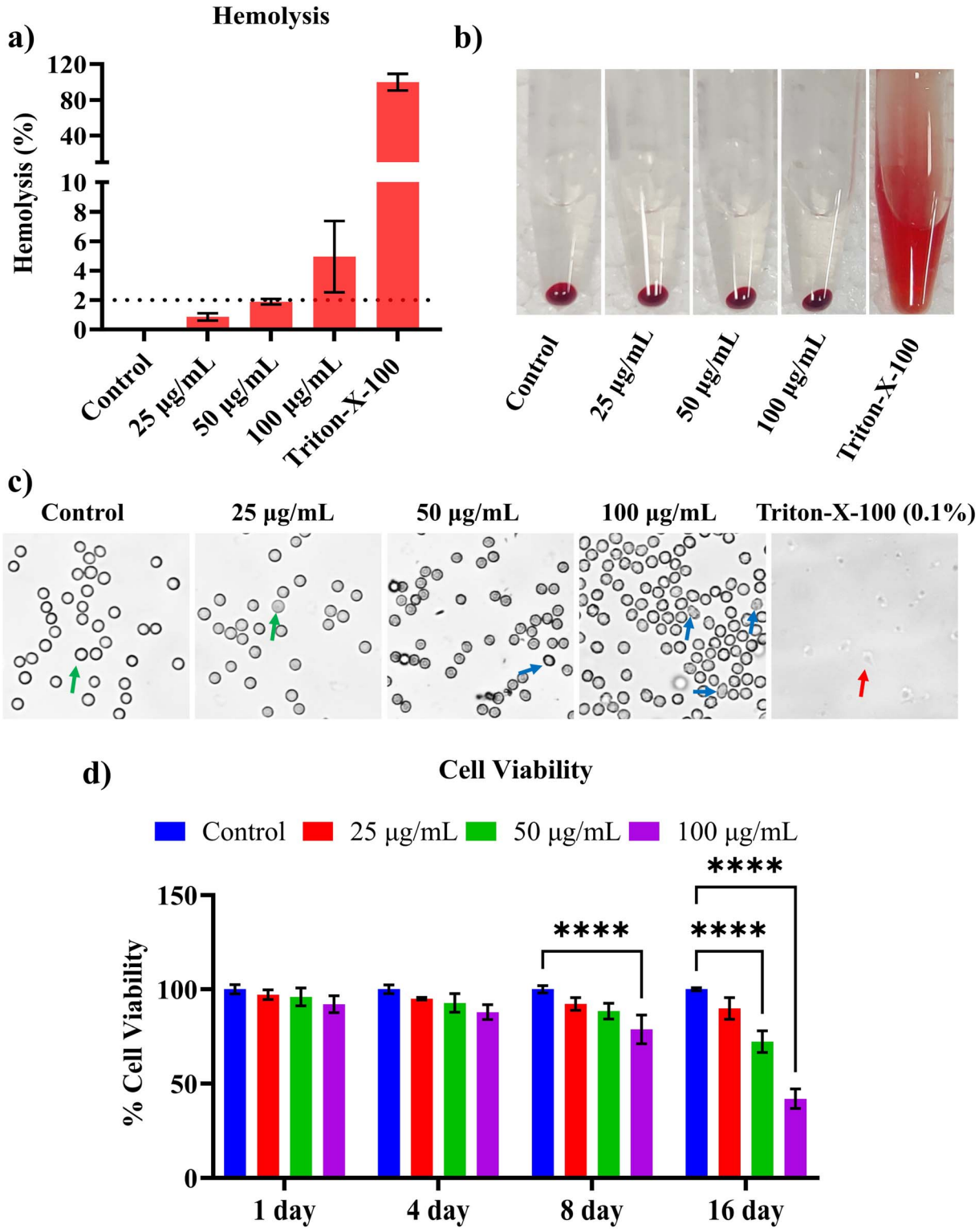

Fig. 6 Hemolysis and cytotoxicity assessment of PBNPs on red blood cells (RBCs) and A549 cells, respectively. (a) Hemolysis percentage of RBCs at different PBNP concentrations. (b) Visual representation of hemolysis in RBC suspensions. (c) Microscopic images of RBC morphology after PBNPs treatment. (d) Viability assay of A549 cells after PBNPs exposure.

3.3.2. Effects on cell viability. The cytotoxicity of nanoplastics (PBNPs) was evaluated at multiple time points: short-term (1 day) and long-term (after 4, 8, and 16 days of exposure to PBNPs). Fig. 6d shows that after 1 day or 24 hours of exposure, no significant reduction in cell viability was observed for PBNPs concentrations up to 100 μg mL^{-1}, indicating that short-term exposure had minimal cytotoxic effects. However, long-term exposure resulted in dose- and time-dependent

cytotoxicity. Notably, by the 8th day, significant reductions in cell viability were observed at concentrations of 100 μg mL^{-1}. This trend became more pronounced by the 16th day, with 50 and 100 μg mL^{-1} concentrations indicating a drastic and statistically significant decline in the cell viability. These findings suggest that prolonged exposure to PBNPs significantly compromises the cell viability, particularly at higher concentrations.

3.3.3. Effects on cellular DNA. The comet assay was performed to evaluate the genotoxic effects of PBNPs on A549 cells after 16 days of exposure. Representative images (Fig. 7a) reveal that the control cells exhibited negligible DNA damage, as evidenced by minimal comet formation. Cells exposed to 50 μg mL^{-1} PBNPs showed the instances of DNA damage but it was not statistically significant as compared to the control group. However, exposure to 100 μg mL^{-1} PBNPs induced a marked increase in comet formation, indicating a significant DNA damage at this concentration.

Quantitative analysis of the comet parameters revealed that the comet length (Fig. 7b) and tail length (Fig. 7c) were significantly increased only at 100 μg mL^{-1} PBNPs, while the 50 μg mL^{-1} group remained statistically comparable to the control. Similarly, the percentage of tail DNA (Fig. 7d) was significantly elevated in the 100 μg mL^{-1} group compared to both the control and 50 μg mL^{-1} groups, reflecting increased DNA fragmentation. Conversely, the percentage of head DNA (Fig. 7e) was significantly reduced in the 100 μg mL^{-1} group, indicating the migration of DNA fragments into the comet tail. These results suggest that prolonged exposure to PBNPs especially at higher concentrations (100 μg mL^{-1}) induces significant DNA damages in A549 cells.

3.3.4. Impact on gene expression. Gene expression analysis in A549 cells after 16 days of PBNPs exposure revealed significant transcriptional changes in key genes associated with apoptosis, oxidative stress, and inflammatory responses (Fig. 8). Caspase-3, a key executioner of apoptosis, showed a significant ~3-fold upregulation at 50 μg mL^{-1}, which further increased to ~3.5-fold at 100 μg mL^{-1} compared to the control (Fig. 8a). Similarly, *p53*, a tumor suppressor gene involved in DNA damage response and cell cycle regulation, exhibited an approximately ~15-fold increase at 50 μg mL^{-1}, though this upregulation was not statistically significant, whereas at 100 μg mL^{-1}, its expression was significantly elevated by ~45-fold (Fig. 8b).

NRF-2, a transcription factor responsible for regulating antioxidant defense mechanisms, showed a ~4-fold increase at

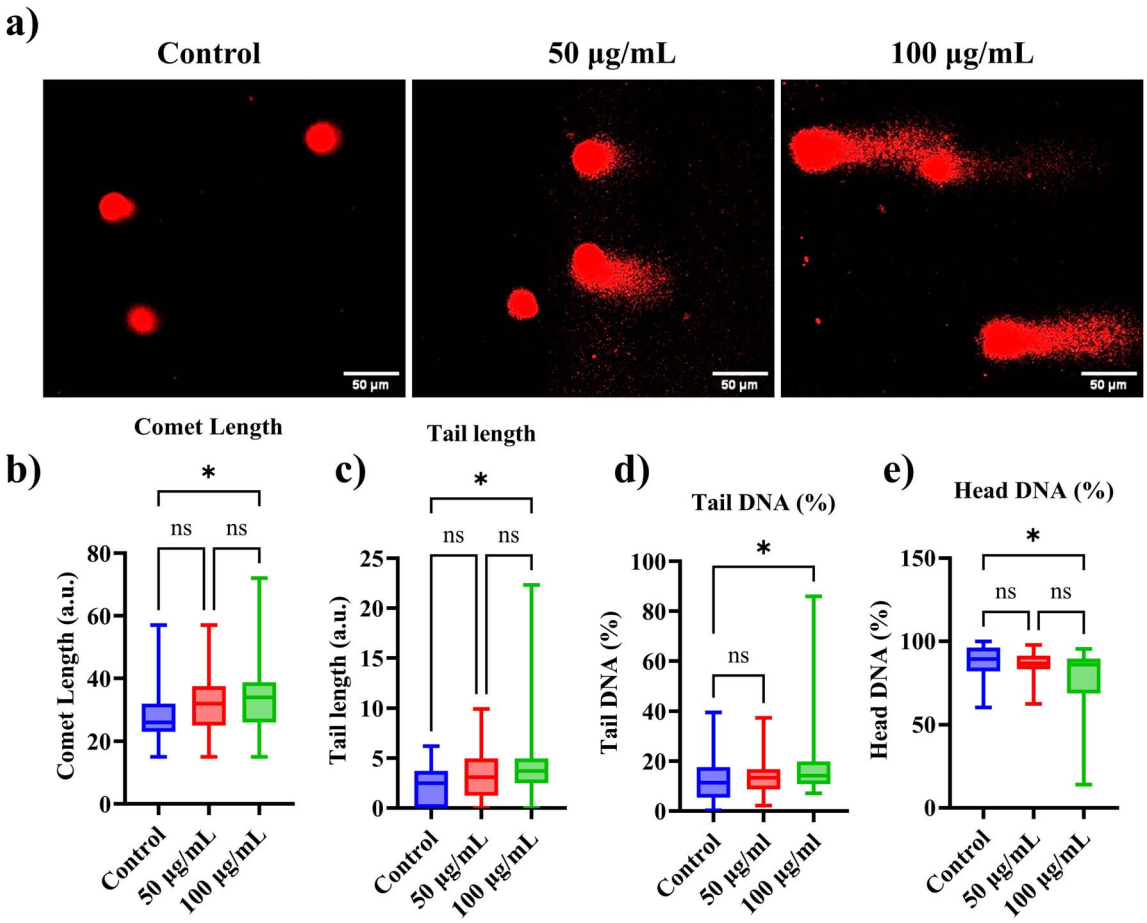

Fig. 7 Comet assay-based analysis of DNA damage in A549 cells after 16 days of exposure to PBNPs. (a) Representative images of comet formation for control, 50 μg mL^{-1}, and 100 μg mL^{-1} PBNPs (scale bar: 50 μm). Quantitative data for (b) comet length, (c) tail length, (d) tail DNA (%), and (e) head DNA (%).

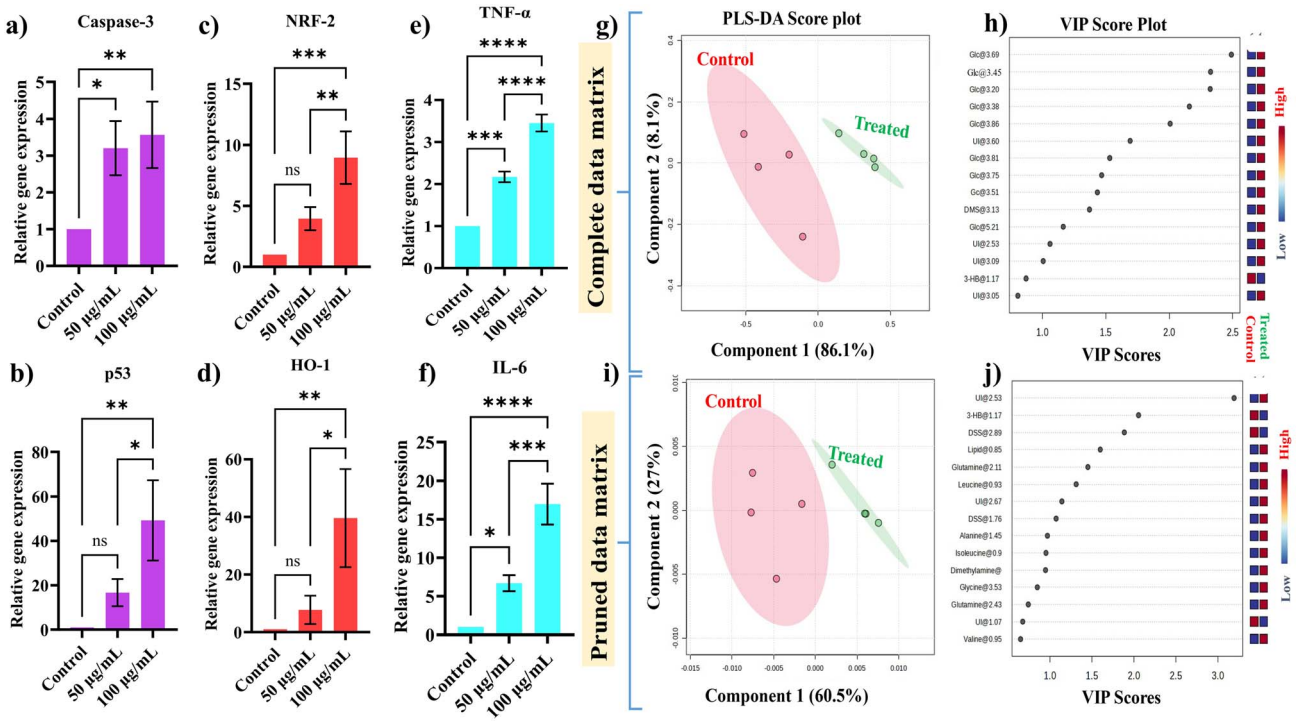

Fig. 8 Gene expression analysis and metabolomic profiling of A549 cells after 16-day exposure to PBNPs. (a and b) Relative expression levels of apoptotic markers Caspase-3 and p53. (c and d) Oxidative stress markers NRF-2 and HO-1. (e and f) Pro-inflammatory cytokines TNF-α and IL-6. (g) PLS-DA score plot for complete data matrix, showing distinct clustering between control (red) and treated (green) groups. (h) VIP score plot for complete data matrix, highlighting key metabolites contributing to group differentiation. (i) PLS-DA score plot for the pruned data matrix, showing distinct clustering between control (red) and treated (green) groups. (j) VIP score plot for the pruned data matrix, highlighting key metabolites contributing to group differentiation.

50 μg mL^{-1}, though this upregulation was not statistically significant. However, at 100 μg mL^{-1}, its expression was significantly elevated by ~8-fold compared to the control (Fig. 8c). HO-1, a downstream target of NRF-2 that plays a crucial role in oxidative stress response and cytoprotection, exhibited a strong dose-dependent increase, with ~10-fold upregulation at 50 μg mL^{-1}, which further rose to ~38-fold at 100 μg mL^{-1} (Fig. 8d).

TNF-α, a pro-inflammatory cytokine involved in immune regulation and cell signaling, was upregulated ~2-fold at 50 μg mL^{-1}, with a further increase to ~3.2-fold at 100 μg mL^{-1} compared to the control (Fig. 8e). Similarly, IL-6, a cytokine that mediates inflammatory responses and plays a role in immune signaling, exhibited a substantial increase, rising ~6-fold at 50 μg mL^{-1} and further reaching ~16-fold at 100 μg mL^{-1} (Fig. 8f).

These results indicate a dose-dependent upregulation of apoptotic, oxidative stress, and inflammatory markers in A549 cells following prolonged exposure to PBNPs, suggesting increased cellular stress with higher concentrations.

3.3.5. Impact on metabolites. The metabolomic profiling of A549 cells exposed to PBNPs (50 μg mL^{-1}) revealed significant alterations in the metabolic landscape between the treated and control groups, as evidenced by PLS-DA and VIP score analyses (Fig. 8g–i). The PLS-DA score plot for the complete data matrix demonstrated clear separation between the two groups, with Component 1 explaining 86.1% of the variance and Component 2 contributing 8.1% (Fig. 8g). Validation metrics for the complete matrix were robust, with R^2 values ranging from 0.83943 to 0.9991 and Q^2 values from 0.72509 to 0.89714, indicating a well-fitted model with strong predictive accuracy. After pruning redundant spectral regions, the pruned data matrix also displayed distinct clustering, with Component 1 accounting for 60.5% of the variance and Component 2 contributing 27% (Fig. 8i). Validation parameters for the pruned matrix, though slightly reduced, were consistent, with R^2 values from 0.8479 to 0.99646 and Q^2 values ranging from 0.50585 to 0.78486, ensuring the reliability of the refined analysis (ESI Fig. 4b†).

The VIP score analysis highlighted critical metabolites driving group separation in both the complete and pruned data matrices. For the complete matrix, glucose-related signals (Glc@3.20, Glc@3.69), and unidentified metabolites (UI@2.53, UI@3.60, UI@3.09) were identified as key contributors, with VIP scores exceeding 1.0 (Fig. 8h). The heatmap on the right shows that glucose levels were increased. In the pruned data matrix, metabolites such as alanine (Alanine@1.45), 3-hydroxybutyrate (3-HB@1.17), lipid (Lipid@0.85), glutamine (Glutamine@2.11), leucine (Leucine@0.93), alanine (Alanin@1.45), isoleucine (Isoleucine@0.9), dimethylamine (Dimethylamine@2.71) and unidentified metabolites (UI@2.67, UI@53) emerged as significant discriminators, refining the understanding of metabolic perturbations caused by PBNPs (Fig. 8j). The heatmap shows

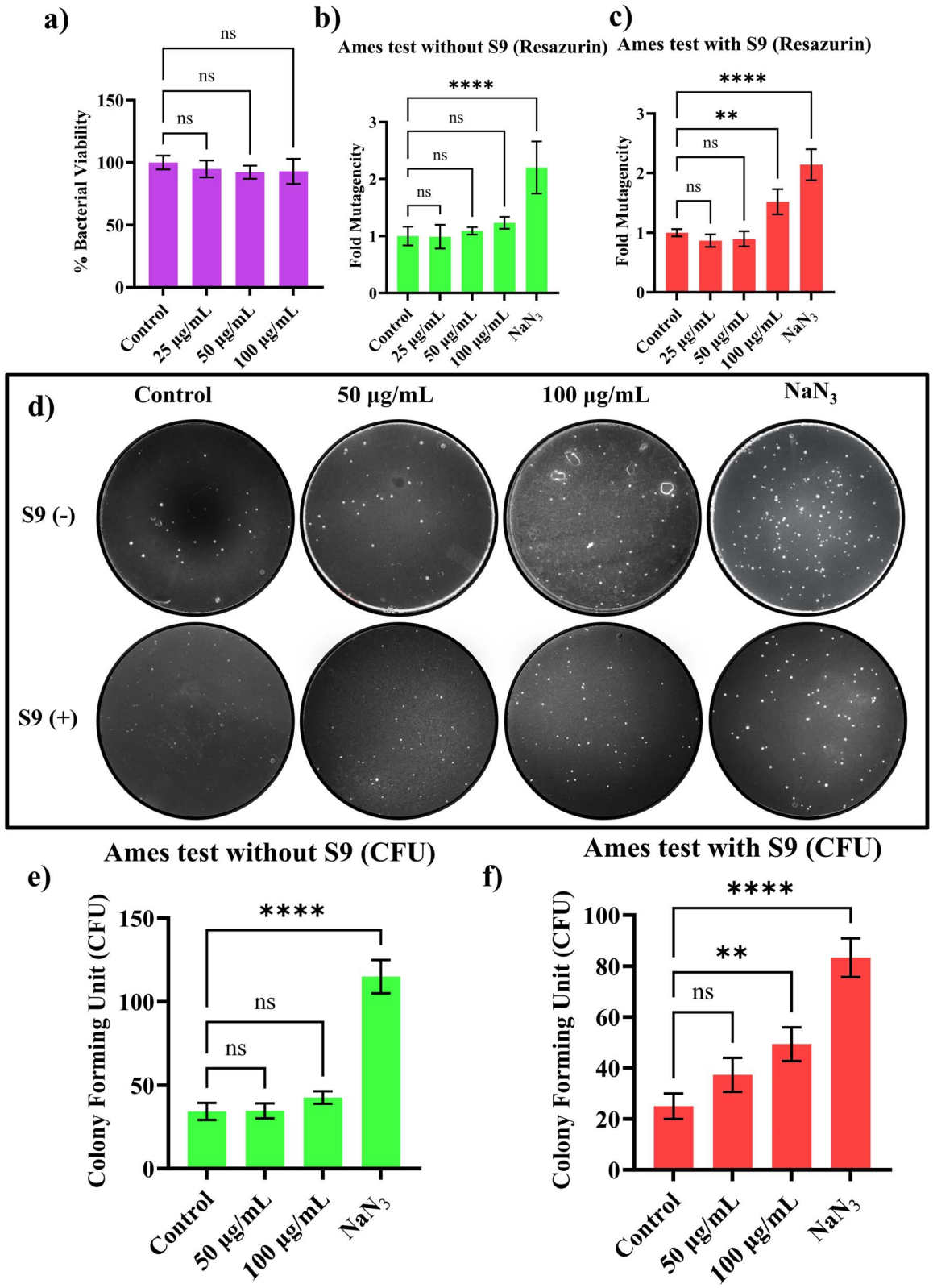

Fig. 9 Ames test assessing the mutagenicity of PBNPs in *Salmonella typhimurium* MTCC 1252 (TA100) strain. (a) Bacterial viability at different PBNP concentrations. (b and c) Fold mutagenicity analyzed using the resazurin assay without S9 (b) and with S9 (c) metabolic activation. (d) Representative agar plates showing colony formation without S9 (top) and with S9 (bottom) activation for control, 50 µg mL^{-1}, 100 µg mL^{-1} PBNPs, and NaN_3 (positive control). (e and f) CFU counts without S9 (e) and with S9 activation (f).

increased levels of alanine, lipid, glutamine, dimethylamine, leucine, and isoleucine, while 3-hydroxybutyrate was decreased. Volcano plot (control with respect to treated) analysis validated these findings, revealing statistically significant downregulation of metabolites such as UI@1.22 and 3-HB@1.17 in the treated samples. Concurrently, metabolites like Dimethylamine@2.71 and Glc@3.69 were significantly upregulated in the treated group. Spectral bin analysis corroborated these results, showing significant metabolic disruptions in glucose (Glc@3.20, Glc@3.69), dimethylamine and amino acid metabolism (*e.g.*, glutamine). Key spectral bins exhibited significant changes based on their $-\log 10\,(\mathrm{FDR}\cdot p)$ values, confirming the impact of PBNPs on energy, nitrogen and amino acid metabolism in A549 cells (ESI Fig. 8†).

3.3.6. Mutagenic potential. The Ames test was employed to evaluate the mutagenic potential of PBNPs in *Salmonella typhimurium* MTCC 1252 (TA100) strain under two experimental conditions: with and without S9 metabolic activation. As an initial step, bacterial viability (Fig. 9a) was assessed to ensure that PBNPs do not induce cytotoxic effects that might compromise the bacterial strain's ability to replicate or participate in the mutagenicity assay. This screening step confirmed the compatibility of PBNPs with the bacterial system across all tested concentrations (25 μg mL^{-1}, 50 μg mL^{-1}, and 100 μg mL^{-1}). The percentage viability remained consistent with the control group, indicating that the observed results in subsequent mutagenicity tests were not influenced by PBNPs toxicity but rather by its mutagenic effects. Mutagenicity screening using the resazurin assay showed distinct outcomes in the presence and absence of S9 metabolic activation. Without S9 activation (Fig. 9b), fold mutagenicity at all concentrations of PBNPs was comparable to the control, indicating no direct mutagenic activity. In contrast, with S9 metabolic activation (Fig. 9c), a significant increase in fold mutagenicity was observed at 100 μg mL^{-1} PBNPs, suggesting that metabolic conversion of PBNPs may produce mutagenic intermediates. The results were further corroborated by agar plate assays (Fig. 9d). In the absence of S9 (top row), colony formation remained consistent across PBNPs concentrations and the control group. However, in the presence of S9 (bottom row), a marked increase in the number of colonies was observed at 100 μg mL^{-1} PBNPs, supporting the mutagenic potential of PBNPs upon metabolic activation. Colony-forming unit (CFU) counts (Fig. 9e and f) quantitatively confirmed these findings. Without S9 activation (Fig. 9e), CFU counts did not differ significantly across treatments. With S9 activation (Fig. 9f), a significant increase in CFU counts was observed at 100 μg mL^{-1} PBNPs, further confirming mutagenicity upon metabolic activation. The positive control (NaN_3) consistently exhibited elevated CFU counts, validating the accuracy and sensitivity of the assay.

4. Discussion

Plastic pollution represents one of the most pressing environmental crises of our time, with significant impacts on ecosystems, biodiversity, and human health.[3,13] The pervasive use of plastics, particularly single-use items, has led to their accumulation in terrestrial and aquatic systems.[14] Over time, macroplastics degrade into smaller fragments known as microplastics (MPs) and nanoplastics (NPs).[15] Unlike their larger counterparts, NPs possess unique physicochemical properties due to their small size and high surface-area-to-volume ratio, making them highly reactive and capable of penetrating biological barriers.[16,17] NPs, typically defined as plastic particles smaller than 1 μm, pose a more significant threat due to their potential to interact with biological systems at the cellular and molecular levels.[18,19] Their widespread distribution in oceans, rivers, soils, and even the atmosphere highlights the urgent need to understand their behavior, toxicity, and interactions with microbiota. To explore the effects of NPs on living systems, this study focused on PET bottle derived NPs, which are commonly released from daily use products such as water bottles and food containers. PET is one of the most widespread plastic pollutants in the environment,[20,21] making it a highly relevant choice for investigating potential biological impacts. Although real-life exposure involves a complex mix of different plastic types and co-contaminants, focusing on a single, well-defined type allows for clearer insight into how these materials interact with biological systems. The exposure doses (0, 25, 50, and 100 μg mL^{-1}) and duration (16 days) were selected based on previous studies conducted in our lab along with several other toxicological research and environmental reports.[12,22–27] Instead of modelling acute high-dose exposures, our study design was aimed to reflect slow, continuous and prolonged exposure of NPs over time, which is something more representative of how organisms are exposed to NPs in their natural surroundings.

To study NPs effects, we utilized a robust method for the synthesis and characterization of NPs (PBNPs) to ensure consistency and relevance to environmental conditions. The PBNPs were synthesized using an oil-in-water nano-emulsion technique, which enabled precise control over size distribution within the nanoscale range while minimizing contamination risks. The method achieved a synthesis yield of approximately 15% (±2%), based on the average dry weight obtained from three independently prepared batches. Subsequent characterization through techniques such as Dynamic Light Scattering (DLS), Field Emission Scanning Electron Microscopy (FESEM), Transmission Electron Microscopy (TEM), and Atomic Force Microscopy (AFM) revealed that the synthesized PBNPs possessed an average size of approximately 280–320 nm, with size distribution from 50 nm to 850 nm, closely mimicking environmental NPs.[12]

To provide a more complete understanding of how NPs affect biological systems, this study employed a multi-model approach involving three different biologically relevant systems: *L. rhamnosus* (a well-studied probiotic strain reflecting gut microbiota), red blood cells (representing blood interaction and membrane-level toxicity), and A549 human epithelial cells (to explore cellular stress responses). This combined framework reflects the layered and realistic path that ingested NPs may follow in the body. Initially, NPs encounter gut bacteria, organisms critical for maintaining microbial balance and overall health. If absorbed, these particles can enter the

bloodstream and interact with red blood cells, which are highly sensitive to membrane disruption. From there, they may reach epithelial tissues, where they can trigger cellular stress, oxidative damage, or other toxic effects. Rather than analyzing each model in isolation, evaluating these interconnected systems together allows for a broader, more contextual view of NPs toxicity. This approach not only captures specific effects at each biological level but also reveals how these effects may relate or build upon one another. It strengthens the mechanistic understanding of NPs' potential risks in a more holistic and biologically meaningful way, something often overlooked in traditional, single-system toxicological studies.

4.1. Nanoplastics and *L. rhamnosus*: a threat to probiotic efficacy

L. rhamnosus is one of the most widely studied probiotic bacteria, known for its key role in supporting gut health.[28] It helps maintain the intestinal barrier, suppress harmful pathogens, and modulate immune responses—functions that are essential for a healthy and balanced gut microbiome.[29] Because of these well-established benefits, *L. rhamnosus* is commonly used in probiotic supplements and functional foods. In this study, we selected *L. rhamnosus* as a representative model to explore how NPs exposure might impact beneficial gut microbes.

The disruption of probiotic functionality in *L. rhamnosus* upon exposure to PBNPs underscores a critical challenge in microbial resilience against NPs-induced stress. A progressive decline in bacterial viability was observed over a 16-day exposure period, exhibiting a concentration-dependent effect where higher doses (50 μg mL^{-1} and 100 μg mL^{-1}) caused substantial reductions. Even at lower concentrations, prolonged exposure gradually compromised bacterial defenses, highlighting the cumulative nature of NPs stress. This effect is primarily attributed to oxidative stress, as evidenced by increased ROS generation and direct interactions with bacterial cells.[30,31] Confocal microscopy revealed a dose-dependent escalation in membrane permeability, as indicated by increased propidium iodide signal, suggesting compromised membrane integrity. Complementary FESEM imaging further corroborated these findings, illustrating distinct morphological alterations such as enlarged bacterial size indicative of stress-induced perturbations in cell structure and metabolic activity.[32]

In response to PBNPs-induced stress, *L. rhamnosus* exhibited a distinct adaptive strategy involving upregulation of *groEL*, a molecular chaperone crucial for mitigating protein misfolding associated with membrane disruption.[33] Additionally, bacterial adaptation mechanisms were evident through enhanced biofilm formation and autoaggregation, suggesting a shift towards protective strategies under persistent stress conditions.[34,35] The increase in biofilm production likely serves as a defense mechanism to counteract oxidative damage, while enhanced autoaggregation facilitates bacterial clustering, thereby promoting surface attachment. Gene expression analysis further supported these observations, with upregulated *dltA* indicating modifications in teichoic acid composition, a critical determinant of biofilm structural stability.[36,37] Concurrent upregulation of *mapA*, a gene implicated in bacterial adherence, suggests a potential compensatory mechanism to reinforce colonization within biofilm matrices, despite overarching stress-induced impairments.[38]

A deeper insight into metabolic adaptations reveals significant shifts in the energy utilization and stress response pathways. Upregulation of *lacF*, a gene central to lactose metabolism and ATP generation, suggests a metabolic reprogramming strategy aimed at sustaining energy homeostasis amidst oxidative stress.[39] However, this adaptation appears to be insufficient in countering ROS-mediated damage, as reflected by impaired antioxidant defenses. Reduced DPPH scavenging activity and downregulation of *trxA*, a gene encoding thioredoxin A, indicate a compromised ability to neutralize oxidative stress, exacerbating cellular damage.[40,41] This imbalance likely directs bacterial survival strategies towards biofilm-mediated protection rather than direct ROS neutralization, reinforcing the observed phenotypic shifts.[42]

A particularly striking observation was the increased susceptibility of *L. rhamnosus* to antibiotics following PBNPs exposure, as evidenced by expanded inhibition zones for multiple antibiotics. This suggests that PBNPs-induced alterations in membrane permeability or metabolic pathways may render bacterial cells more vulnerable to antimicrobial agents.[43,44] Additionally, a significant decline in probiotic traits was observed, including reduced adherence to HCT 116 colon epithelial cells and diminished antibacterial activity. Interestingly, despite *mapA* upregulation, oxidative stress likely compromises protein functionality, leading to impaired adhesion and colonization potential.[45] Structural damage at the protein and lipid levels may underlie this dysfunction, ultimately attenuating the bacterium's ability to exert beneficial effects.[46]

Metabolomic analysis further substantiates the extensive perturbations induced by PBNPs exposure, revealing disruptions in fundamental pathways governing energy metabolism and amino acid biosynthesis. These findings collectively highlight the profound impact of NPs on probiotic bacterial physiology, emphasizing their potential to destabilize microbial homeostasis and compromise probiotic efficacy through oxidative stress, metabolic reprogramming, and membrane perturbation.

These findings are especially important because they highlight more than just a reduction in probiotic survival. Results show that NPs can interfere with how probiotics function and interact within their environment, including with the host and other microbes in the gut. Critical probiotic traits such as adhesion to gut surfaces, antioxidant, and antibacterial activity were all significantly disrupted. These traits are common across many beneficial gut bacteria.[47,48] This suggests that the negative effects observed here could extend to a broader group of probiotic species. If these core functions are impaired, it could disturb the balance of the gut microbiome and reduce its ability to recover from stress or maintain overall health. In this way, NPs may not only affect individual microbial cells but also compromise the stability and resilience of the entire gut

ecosystem. These insights deepen our understanding of how NPs disrupt essential microbial and cellular functions. More importantly, they point to real-world consequences, such as reduced probiotic effectiveness and compromised gut health. Given the growing presence of NPs in our environment and food systems, these results underscore the urgent need for more detailed risk assessments and the development of strategies to minimize their biological impact.

4.2. Nanoplastics and mammalian cells: unmasking the cytotoxic threat

To assess the broader implications of NPs exposure on human health, we selected A549 cells, a widely used epithelial cell line derived from the human alveolar epithelium. A549 cells are extensively used in nanotoxicology research due to their stable epithelial phenotype, robust growth characteristics, and well-characterized responses to oxidative and inflammatory stress.[49–53] Importantly, these cells express functional p53 and maintain epithelial features such as tight junctions and metabolic activity, making them a practical and reproducible *in vitro* model for evaluating cellular-level toxicity.[54,55] A549 cells are a relevant and validated model for general cytotoxicity, mechanistic stress responses, and oxidative injury pathways, especially when the goal is to establish foundational toxicological insights.[49–53]

Our findings show that exposure to PBNPs induced a clear dose- and time-dependent cytotoxic effect in A549 cells. Short-term exposure to lower concentrations exhibited minimal effects on cell viability, suggesting initial tolerance. However, prolonged exposure led to a marked decline in viability, highlighting the cumulative stress induced by PBNPs over time. These findings raise concerns about chronic environmental exposure, particularly in scenarios where NPs accumulation is sustained. Beyond cytotoxicity, hemolysis assays provided insights into the interaction between PBNPs and red blood cells. While lower concentrations exhibited general hemocompatibility, exposure at 50 μg mL^{-1} resulted in morphological changes, and at 100 μg mL^{-1}, pronounced membrane disruption and cell shrinkage were evident. These structural alterations suggest potential physical or chemical interactions with cell membranes, which could have implications for circulatory health.[56] Genotoxicity assessments further substantiated the adverse effects of PBNPs, particularly at higher concentrations. The comet assay revealed significant DNA damage, as indicated by increased comet tail length and tail DNA percentage. The oxidative stress-mediated nature of this damage was supported by the upregulation of NRF-2 and HO-1, key regulators of antioxidant defense mechanisms.[57,58] This oxidative imbalance was further reinforced by metabolomic analysis, which revealed disruptions in energy metabolism and amino acid pathways, indicating metabolic stress.

Molecular-level changes further illustrated the cellular response to PBNP exposure. A dose-dependent upregulation of apoptotic markers, including Caspase-3 and p53, indicated the activation of programmed cell death pathways. Simultaneously, the increase in pro-inflammatory markers TNF-α and IL-6 suggested a significant inflammatory response, aligning with the observed oxidative stress and cytotoxicity. The convergence of these molecular events underscores the potential of PBNPs to compromise cellular homeostasis.[59,60]

Metabolomic profiling further highlighted substantial shifts in key metabolic pathways. Alterations in glucose, alanine, glutamine, and dimethylamine levels distinguished treated cells from controls, suggesting a metabolic reprogramming response to counteract PBNPs-induced stress. These biochemical shifts align with cytotoxic and gene expression data, reinforcing the notion that PBNPs impose a significant metabolic burden on exposed cells.

Ames test results provided additional evidence of PBNPs-induced genotoxicity, revealing mutagenic activity upon metabolic activation (S9). This suggests that metabolic intermediates of PBNPs may pose an even greater genetic risk than the parent material. Combined with the comet assay findings, these results indicate the carcinogenic abilities of NPs especially in cases of long term exposures, however, further investigations are warranted to fully understand the effects on long-term genetic stability and potential mutagenic risks associated.

These results reveal that NPs can profoundly disrupt fundamental cellular processes in human epithelial systems. The combination of oxidative stress, DNA damage, metabolic imbalance, and pro-inflammatory signaling observed in A549 cells indicates that these particles trigger a multifaceted stress response with potential implications for tissue health and systemic physiology. Given that such stress pathways are conserved across various human cell types, these findings raise broader concerns about how chronic or repeated exposure to NPs might influence organ functions—particularly in the lungs, where inhaled particles are likely to accumulate. Disruptions in apoptosis regulation, antioxidant defense, and metabolic activity may collectively impair cellular resilience and increase vulnerability to inflammatory or degenerative diseases. These cellular-level disturbances do not operate in isolation; over time, they may contribute to cumulative biological stress with long-term health consequences. The study emphasizes that NPs are not just passive contaminants but active biological stressors, capable of altering critical molecular and metabolic pathways.

4.3. Possible mechanisms underlying nanoplastics toxicity across cellular models and their implications

NPs, because of their nanoscale size can easily traverse across biological barriers, allowing them to reach multiple tissues and cell types, raising significant concerns about their widespread and long-term effects on human health. This study employed a tripartite experimental model comprising gut microbiome, RBCs, and human epithelial cells to better understand the effects of NPs. Despite vast biological differences among these systems in terms of origin, structure, and function, each model exhibited remarkably adverse responses to NPs exposure, including morphological alterations in RBCs, DNA damage, loss of viability, gene expression perturbations, and metabolic changes in A549 cells, and membrane integrity disruption, viability loss, gene

expression changes, morphological damage, and metabolic shifts in bacteria. Such cross-model evidence of cellular disruption suggests that NPs do not merely cause cell-specific injuries, but rather interfere with foundational cellular processes that are universally critical to biological survival—namely redox regulation, bioenergetics, and membrane stability.[61–63] These processes are conserved across evolutionary lineages,[64–67] making them vulnerable common targets of toxicants particularly the nanoscale materials. The consistent induction of oxidative stress across all models, for instance, highlights NPs' potential to disrupt the intracellular redox balance, leading to macromolecular damage, energy failure, and ultimately, cell dysfunction or death.[68] Moreover, alterations in membrane architecture observed in both prokaryotic and eukaryotic models point to direct physicochemical interactions between plastic particles and lipid bilayers—disrupting permeability, transport functions, and cellular signalling.

Importantly, these findings should not be viewed in isolation. While each model was studied separately, the correlation of outcomes across systems reveals mechanistic continuity, providing insight into how NPs may behave in the human body under real-world conditions. For instance, gut dysbiosis due to microbial oxidative stress and membrane disruption may impair metabolite production, impacting host immunity and metabolic regulations.[69,70] These effects may, in turn, influence circulating RBCs, altering redox balance and releasing damage-associated molecular patterns (DAMPs), which can activate inflammatory responses in distant epithelial tissues.[71] Similarly, stress signals originating from epithelial cells exposed to NPs could lead to cytokine production that feeds back into the gut or bloodstream, altering microbiota composition or RBC stability.[72] Thus, although these models were assessed independently, the shared molecular disruptions and their physiological interdependencies support the concept of a systemic cascade of NPs toxicity.

5. Conclusion

This study provides comprehensive insights into the toxicological and metabolic effects of PBNPs on both microbial and mammalian systems, revealing significant disruptions in cellular homeostasis, metabolic pathways, and overall functionality. The findings demonstrate that prolonged exposure to PBNPs adversely affects the probiotic bacterium *L. rhamnosus*, leading to a decline in bacterial viability, impaired growth kinetics, and compromised membrane integrity. The observed increase in biofilm formation and autoaggregation, along with altered antibiotic susceptibility and reduced adherence to human colon epithelial cells, suggests that NPs may interfere with probiotic stability and gut colonization. These disruptions could have profound implications for host–microbe interactions, potentially affecting gut microbiota composition, intestinal barrier integrity, and overall health. Metabolomic analysis of *L. rhamnosus* exposed to PBNPs revealed significant disruptions in glucose and lactate metabolism, along with alterations in amino acid and membrane lipid metabolism, indicating metabolic stress and adaptive responses that may impair probiotic functionality.

In mammalian A549 epithelial cells, PBNPs elicited significant cytotoxicity, genotoxicity, oxidative stress, and inflammatory responses, particularly after prolonged exposure. While short-term exposure did not cause substantial effects, long-term exposure resulted in dose-dependent reductions in cell viability and DNA integrity. The upregulation of apoptotic markers (Caspase-3, p53) and oxidative stress regulators (NRF-2, HO-1) indicates that NPs exposure induces cellular stress responses that may contribute to long-term physiological disturbances. The activation of pro-inflammatory cytokines (TNF-α, IL-6) further suggests that NPs may exacerbate inflammatory conditions, potentially increasing the risk of chronic diseases. Metabolomic profiling revealed disruptions in key metabolic pathways, including glucose and amino acid metabolism, indicating that NPs exposure leads to metabolic stress and potential energy imbalances. Furthermore, Ames mutagenicity testing showed that PBNPs, when metabolically activated, exhibit significant mutagenic potential, raising concerns about their role in genomic instability and carcinogenesis.

These findings collectively underscore the emerging risks associated with PBNPs as environmental pollutants, highlighting their potential to disrupt microbial ecosystems and pose serious health threats. The adverse effects observed in both bacterial and human cell models emphasize the need for a deeper understanding of the long-term consequences of NPs exposure. Given the widespread presence of NPs in the environment, their interactions with biological systems warrant further investigation, particularly in the context of bioaccumulation, systemic toxicity, and transgenerational effects.

Future research should focus on elucidating the mechanisms underlying NPs-induced toxicity, assessing their impact on gut microbiota–host interactions, and evaluating their potential to contribute to inflammatory diseases, metabolic disorders, and cancer progression. Additionally, regulatory frameworks must be strengthened to address the risks associated with NP contamination, and efforts should be directed toward the development of sustainable materials and mitigation strategies to reduce environmental and human exposure. Addressing these challenges is crucial for safeguarding both ecosystem stability and public health in the face of increasing NP pollution.

Data availability

All data are available in the manuscript and its ESI.†

Author contributions

PS conceptualized the research idea, designed and conducted all experiments, interpreted the results, and drafted the manuscript. SD assisted in performing the experiments. GS and DK contributed to the metabolomics analysis. MS played a key role in conceptualizing the study, supervising the experiments, analyzing the data, writing and reviewing and finalizing the manuscript. All authors read and approved the final version of the manuscript.

Conflicts of interest

The authors have no conflicts of interest.

Acknowledgements

PS is grateful to University Grants Commission (UGC) for fellowship 1013/[CSIR-UGC NET, JUNE 2019]. MS thankfully acknowledges INST Mohali for providing necessary infrastructure and lab facilities. The authors acknowledge Samraggi Choudhury for providing access to her BioRender subscription, which was used to create the graphical illustrations in this study. DK acknowledge the Department of Medical Education, Govt. of Uttar Pradesh and DST SUPREME DST Project DST/SUPREME/2023/70 for supporting the maintenance, functioning and upgradation of High Field 800 MHz state-of-the art NMR spectrometer at Centre of Biomedical Research, Lucknow, India. GS acknowledges the Council of Scientific and Industrial Research (CSIR), New Delhi, India, for his fellowship under CSIR Junior Research Fellowship (SRF) scheme (No. F. 09/0916(14014)/2022-EMR-I).

References

1 J. P. Da Costa, T. Rocha-Santos and A. C. Duarte, *The environmental impacts of plastics and micro-plastics use, waste and pollution: EU and national measures*, European Parliament, 2020.
2 I. E. Napper and R. C. Thompson, *Annu. Rev. Environ. Resour.*, 2023, **48**, 55–79.
3 R. C. Thompson, C. J. Moore, F. S. vom Saal and S. H. Swan, *Philos. Trans. R. Soc. Lond. B Biol. Sci.*, 2009, **364**, 2153–2166.
4 A. L. Andrady and M. A. Neal, *Philos. Trans. R. Soc. Lond. B Biol. Sci.*, 2009, **364**, 1977–1984.
5 L. Zhu, C. Xie, L. Chen, X. Dai, Y. Zhou, H. Pan and K. Tian, *Ecotoxicol. Environ. Saf.*, 2023, **255**, 114818.
6 L. K. Ncube, A. U. Ude, E. N. Ogunmuyiwa, R. Zulkifli and I. N. Beas, *Recycling*, 2021, **6**, 12.
7 Y.-H. V. Soong, M. J. Sobkowicz and D. Xie, *Bioengineering*, 2022, **9**, 98.
8 P. Benyathiar, P. Kumar, G. Carpenter, J. Brace and D. K. Mishra, *Polymers*, 2022, **14**, 2366.
9 L. Shi, X. Teng, C. Wu, T. Zhang, X. Jin, L. Wang, P. Tian, K. Shang, J. Zhao, C. Rao and G. Wang, *Environ. Pollut.*, 2025, **366**, 125288.
10 X. Teng, T. Zhang and C. Rao, *Front. Microbiol.*, 2025, **15**, 1522794.
11 W. Chen, Q. Guo, H. Li, X. Chi, X. Ma, Y. Tang, Q. Liang, Z. Liu, Y. Liu and J. Li, *Adv. Sci.*, 2025, **12**, 2417283.
12 P. Sharma, A. Kishore and M. Singh, *Nanoscale*, 2024, **16**, 21360–21378.
13 C. M. Rochman, E. Hoh, B. T. Hentschel and S. Kaye, *Environ. Sci. Technol.*, 2013, **47**, 1646–1654.
14 R. Geyer, J. R. Jambeck and K. L. Law, *Sci. Adv.*, 2017, **3**, e1700782.
15 A. L. Andrady, *Mar. Pollut. Bull.*, 2011, **62**, 1596–1605.
16 S. L. Wright and F. J. Kelly, *Environ. Sci. Technol.*, 2017, **51**, 6634–6647.
17 R. Lehner, C. Weder, A. Petri-Fink and B. Rothen-Rutishauser, *Environ. Sci. Technol.*, 2019, **53**, 1748–1765.
18 A. F. R. M. Ramsperger, E. Bergamaschi, M. Panizzolo, I. Fenoglio, F. Barbero, R. Peters, A. Undas, S. Purker, B. Giese, C. R. Lalyer, A. Tamargo, M. V. Moreno-Arribas, H.-P. Grossart, D. Kühnel, J. Dietrich, F. Paulsen, A. K. Afanou, S. Zienolddiny-Narui, S. Eriksen Hammer, T. Kringlen Ervik, P. Graff, B. C. Brinchmann, K.-C. Nordby, H. Wallin, M. Nassi, F. Benetti, M. Zanella, J. Brehm, H. Kress, M. G. J. Löder and C. Laforsch, *NanoImpact*, 2023, **29**, 100441.
19 A. Kishore, I. De, P. Sharma and M. Singh, in *Nanobiotechnology: Principles and Applications*, Bentham Science Publishers, 2023, pp. 163–184.
20 S. M. Gettings, W. Timbury, A. Dmochowska, R. Sharma, R. McGonigle, L. E. MacKenzie, G. Miquelard-Garnier and N. Bourbia, *NanoImpact*, 2024, **34**, 100508.
21 Y.-H. V. Soong, M. J. Sobkowicz and D. Xie, *Bioengineering*, 2022, **9**, 98.
22 Z. Manoochehri, M. Etebari, P. Pannetier and K. Ebrahimpour, *J. Toxicol. Environ. Health Sci.*, 2024, **16**, 203–215.
23 J. C. Aguilar-Guzmán, K. Bejtka, M. Fontana, E. Valsami-Jones, A. M. Villezcas, R. Vazquez-Duhalt and A. G. Rodríguez-Hernández, *Microplast. Nanoplast.*, 2022, **2**, 9.
24 I. Barguilla, J. Domenech, S. Ballesteros, L. Rubio, R. Marcos and A. Hernández, *J. Hazard. Mater.*, 2022, **438**, 129470.
25 S. Murugadoss, L. Godderis, M. Ghosh and P. H. Hoet, *Nanomaterials*, 2021, **11**, 1793.
26 J. Domenech, M. de Britto, A. Velázquez, S. Pastor, A. Hernández, R. Marcos and C. Cortés, *Biomolecules*, 2021, **11**, 1442.
27 M. Peng, C. Grootaert, M. Vercauteren, N. Boon, C. Janssen, A. Rajkovic and J. Asselman, *Environ. Sci. Technol.*, 2024, **58**, 9967–9979.
28 J. Feng, Q. Cen, Y. Cui, X. Hu, M. Li, L. Wang, J. Wei, N. Sun, J. Wang and A. Zhang, *Pharmacol. Res.*, 2025, **211**, 107541.
29 J. Feng, Q. Cen, Y. Cui, X. Hu, M. Li, L. Wang, J. Wei, N. Sun, J. Wang and A. Zhang, *Pharmacol. Res.*, 2025, **211**, 107541.
30 P. M. Mafla-Endara, V. Meklesh, J. P. Beech, P. Ohlsson, M. Pucetaite and E. C. Hammer, *Sci. Total Environ.*, 2023, **904**, 166503.
31 I. Donisi, A. Colloca, C. Anastasio, M. L. Balestrieri and N. D'Onofrio, *Int. J. Biol. Sci.*, 2024, **20**, 5779–5792.
32 B. Ahmed, F. Ameen, A. Rizvi, K. Ali, H. Sonbol, A. Zaidi, M. S. Khan and J. Musarrat, *ACS Omega*, 2020, **5**, 7861–7876.
33 L. Goltermann, L. Good and T. Bentin, *J. Biol. Chem.*, 2013, **288**, 10483–10489.
34 L. Li, X. Gao, M. Li, Y. Liu, J. Ma, X. Wang, Z. Yu, W. Cheng, W. Zhang, H. Sun, X. Song and Z. Wang, *Front. Cell. Infect. Microbiol.*, 2024, **14**, 1324895.
35 T. Trunk, H. S. Khalil, J. C. Leo, T. Trunk, H. S. Khalil and J. C. Leo, *AIMS Microbiol.*, 2018, **4**, 140–164.

36 F. Fabretti, C. Theilacker, L. Baldassarri, Z. Kaczynski, A. Kropec, O. Holst and J. Huebner, *Infect. Immun.*, 2006, **74**, 4164–4171.
37 F. Fitzpatrick, H. Humphreys and J. O'gara, *Clin. Microbiol. Infect.*, 2005, **11**, 967–973.
38 A. J. Collins, A. B. Pastora, T. J. Smith and G. A. O'Toole, *J. Bacteriol.*, 2020, **202**, 10–1128.
39 G. N. Bidart, J. Rodríguez-Díaz, G. Pérez-Martínez and M. J. Yebra, *Sci. Rep.*, 2018, **8**, 7152.
40 Z. Liu, *Biophys. Rep.*, 2023, **9**, 26–32.
41 B. Yang, Y. Lin, Y. Huang, Y.-Q. Shen and Q. Chen, *Redox Biol.*, 2024, **70**, 103032.
42 W. S. da Cruz Nizer, M. E. Adams, K. N. Allison, M. C. Montgomery, H. Mosher, E. Cassol and J. Overhage, *Biofilm*, 2024, **7**, 100203.
43 J. M. Stokes, A. J. Lopatkin, M. A. Lobritz and J. J. Collins, *Cell Metab.*, 2019, **30**, 251–259.
44 A. H. Delcour, *Biochim. Biophys. Acta*, 2009, **1794**, 808–816.
45 A. J. Collins, A. B. Pastora, T. J. Smith and G. A. O'Toole, *J. Bacteriol.*, 2020, **202**(18), e00277.
46 T. Feng and J. Wang, *Gut Microbes*, 2020, **12**, 1801944.
47 R. Wang, Y. Liu, Y. Wen, S. Chen, X. Zhang, C. Zhang and X. Liu, *Trends Food Sci. Technol.*, 2025, **159**, 104945.
48 T. Aziz, H. Xingyu, A. Sarwar, M. Naveed, M. A. Shabbir, A. A. Khan, T. Ulhaq, M. Shahzad, Y. Zhennai and A. Shami, *Front. Microbiol.*, 2023, **14**, 1265188.
49 L. Bobyk, A. Tarantini, D. Beal, G. Veronesi, I. Kieffer, S. Motellier, E. Valsami-Jones, I. Lynch, P.-H. Jouneau, K. Pernet-Gallay, C. Aude-Garcia, S. Sauvaigo, T. Douki, T. Rabilloud and M. Carriere, *Environ. Sci.: Nano*, 2021, **8**, 806–821.
50 M. Xu, G. Halimu, Q. Zhang, Y. Song, X. Fu, Y. Li, Y. Li and H. Zhang, *Sci. Total Environ.*, 2019, **694**, 133794.
51 L. Armand, A. Tarantini, D. Beal, M. Biola-Clier, L. Bobyk, S. Sorieul, K. Pernet-Gallay, C. Marie-Desvergne, I. Lynch and N. Herlin-Boime, *Nanotoxicology*, 2016, **10**, 913–923.
52 N. Nazemof, D. Breznan, Y. Dirieh, E. Blais, L. J. Johnston, A. F. Tayabali, J. Gomes and P. Kumarathasan, *Nanomaterials*, 2024, **14**, 1601.
53 M. Xu, G. Halimu, Q. Zhang, Y. Song, X. Fu, Y. Li, Y. Li and H. Zhang, *Sci. Total Environ.*, 2019, **694**, 133794.
54 M. Biola-Clier, D. Beal, S. Caillat, S. Libert, L. Armand, N. Herlin-Boime, S. Sauvaigo, T. Douki and M. Carriere, *Mutagenesis*, 2017, **32**, 161–172.
55 L. Bobyk, A. Tarantini, D. Beal, G. Veronesi, I. Kieffer, S. Motellier, E. Valsami-Jones, I. Lynch, P.-H. Jouneau, K. Pernet-Gallay, C. Aude-Garcia, S. Sauvaigo, T. Douki, T. Rabilloud and M. Carriere, *Environ. Sci.: Nano*, 2021, **8**, 806–821.
56 R. Sharma and A. Jain, *Pediatr. Hematol. Oncol. J.*, 2024, **9**, 65–73.
57 Q. Ma, *Annu. Rev. Pharmacol. Toxicol.*, 2013, **53**, 401–426.
58 C. Russo, M. Acito, C. Fatigoni, M. Villarini and M. Moretti, *Int. J. Environ. Res. Public Health*, 2020, **17**, 9234.
59 A. Le, A. N. Lane, M. Hamaker, S. Bose, A. Gouw, J. Barbi, T. Tsukamoto, C. J. Rojas, B. S. Slusher, H. Zhang, L. J. Zimmerman, D. C. Liebler, R. J. C. Slebos, P. K. Lorkiewicz, R. M. Higashi, T. W. M. Fan and C. V. Dang, *Cell Metab.*, 2012, **15**, 110–121.
60 M. Holeček, *Int. J. Mol. Sci.*, 2024, **25**, 7037.
61 D. Trachootham, W. Lu, M. A. Ogasawara, N. R.-D. Valle and P. Huang, *Antioxid. Redox Signaling*, 2008, **10**, 1343–1374.
62 S. T. Decker and K. Funai, *Cell Metab.*, 2024, **36**, 1963–1978.
63 Y. Peng and B. Chen, *Virulence*, 2023, **15**, 2299183.
64 J. Santolini, S. A. Wootton, A. A. Jackson and M. Feelisch, *Curr. Opin. Physiol.*, 2019, **9**, 34–47.
65 H. Sies, R. J. Mailloux and U. Jakob, *Nat. Rev. Mol. Cell Biol.*, 2024, **25**, 701–719.
66 C. Dias and J. Nylandsted, *Cell Discovery*, 2021, **7**, 4.
67 T. M. Iverson, *Curr. Opin. Chem. Biol.*, 2006, **10**, 91–100.
68 A. Manke, L. Wang and Y. Rojanasakul, *BioMed Res. Int.*, 2013, **2013**, 942916.
69 H. Mostafavi Abdolmaleky and J.-R. Zhou, *Antioxidants*, 2024, **13**, 985.
70 Y. Zhang, R. Chen, D. Zhang, S. Qi and Y. Liu, *Biomed. Pharmacother.*, 2023, **160**, 114295.
71 R. Mendonça, A. A. A. Silveira and N. Conran, *Inflammation Res.*, 2016, **65**, 665–678.
72 J. C. Onyiah and S. P. Colgan, *Cell. Mol. Life Sci.*, 2016, **73**, 4203–4212.